Identification and characterization of a ribose 2′-O-methyltransferase encoded by the ronivirus branch of Nidovirales

Article

Accepted Version

Figures to accompany the text

Identification and Characterization of a Ribose 2′-O-Methyltransferase encoded by the ronivirus branch of *Nidovirales*

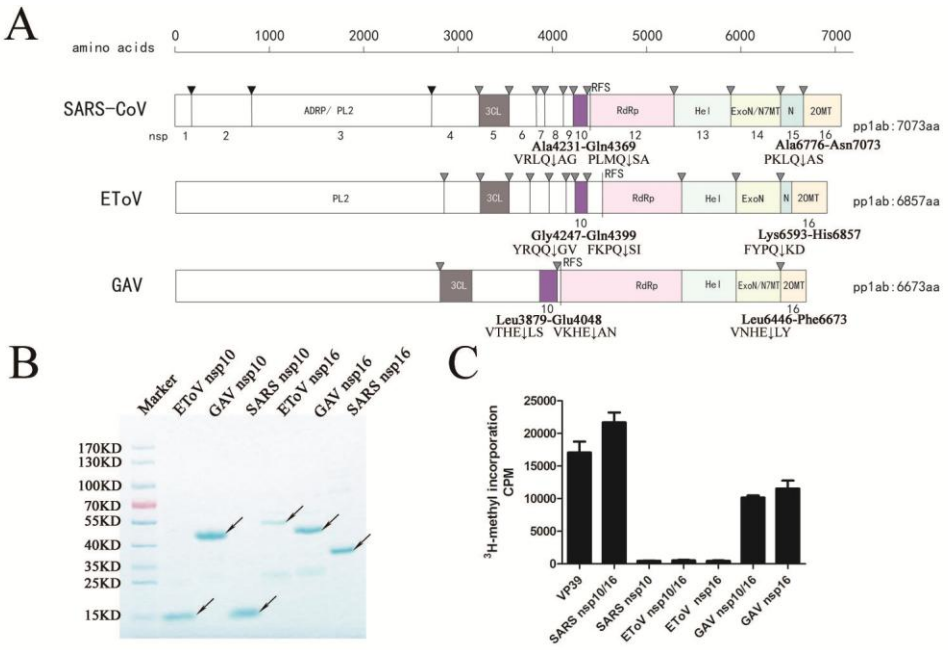

Figure 1. Identification of nidovirus 2′-O-MTases. (A) Domain organization of the replicase pp1ab polyprotein for selected nidoviruses: SARS-CoV (coronavirus), EToV (torovirus) and GAV (ronivirus). the predicted domains are indicated, and the cleavage sites are marked with triangles. The domains include: ADRP, ADP-ribose-1′-phosphatase; PLpro, papain-like proteinases; 3CLpro, chymotrypsin-like proteinase; RdRp, RNA-dependentRNA polymerase ; Hel, helicase; ExoN, exonuclease; N7MT, N7-methyltransferase; Ne, uridylate-specific endoribonuclease (also abbreviated NendoU); 2OMT, 2′-O-methyltransferase. The coronavirus nsp10 and its similarly located counterparts in EToV and GAV are depicted in purple color, and RFS stands for the ribosomal frameshift site. (B) Expression and purification of recombinant viral proteins. The gels of SDS-PAGE were stained with Coomassie brilliant blue. Lanes 2-7 are EToV nsp10, GAV nsp10, SARS nsp10, EToV nsp16, GAV nsp16 and SARS nsp16, respectively. GAV nsp10, GAV nsp16 and EToV nsp16 are GST fusion proteins, and the others are 6-histidine-tagged. (C) The activity assays of potential 2′-O methyltransferases in ^{3}H-methyl incorporation assay. Vaccinia virus VP39 and SARS-CoV nsp10/16 were used as positive control, while SARS-CoV nsp10 acted as a negative control for 2'-O-MTase activity. The CPM amounts reflect the 2′-O-MTase activity which was detected by liquid scintillation.

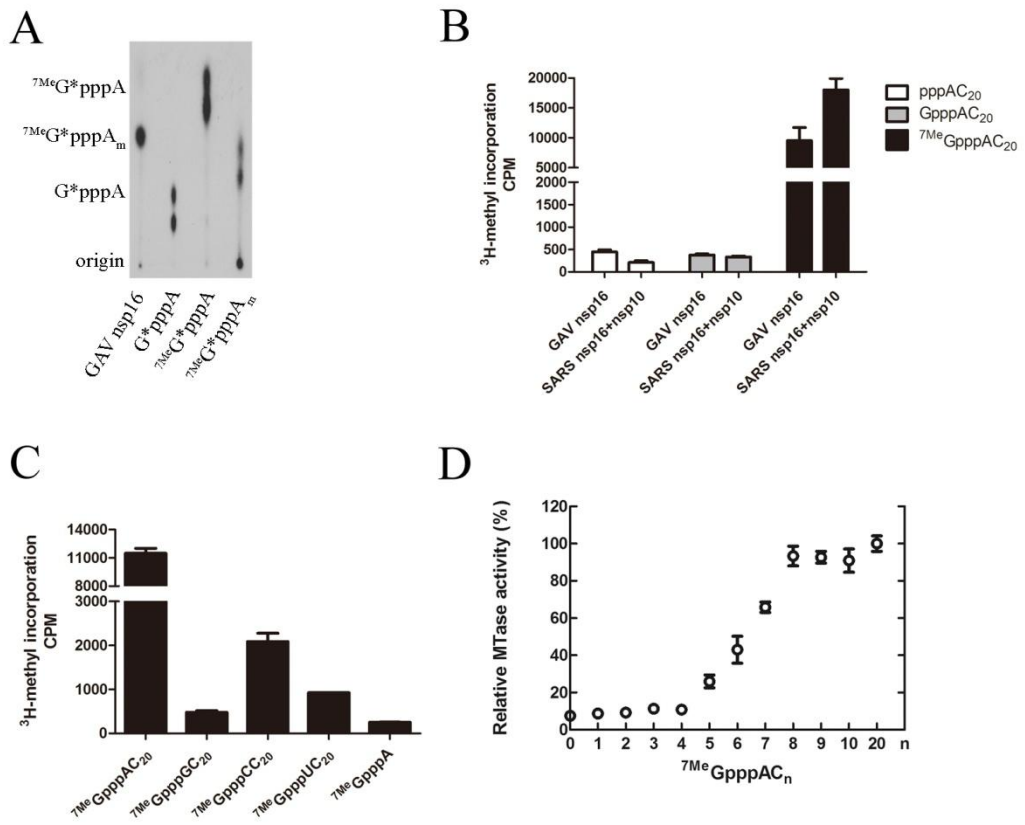

Figure 2. RNA substrate specificity of GAV nsp16 2'-O-MTase. (A) The first 68 nucleotides of the GAV genome was capped to form ^{7Me}G*pppA-RNA, incubated with GAV nsp16, digested to release cap structures, and analyzed by TLC. (B) SAM-dependent methyltransferase activity of GAV nsp16 and SARS nsp16. Equal amounts of proteins were incubated with AC_{20} (white), $GpppAC_{20}$ (gray) and $^{7Me}GpppAC_{20}$ (black) in the presence of ^{3}H-labeled SAM for 1 h, and radioactive incorporation was detected by liquid scintillation. (C) MTase activity of GAV nsp16 for capped RNAs with different initiating nucleotide. $^{7Me}GpppAC_{20}$, $^{7Me}GpppCC_{20}$, $^{7Me}GpppUC_{20}$, $^{7Me}GpppGC_{20}$ and $^{7Me}GpppA$ were used as substrates to test GAV nsp16 activity. (D) GAV nsp16 2′-O-MTase activity on capped RNA substrates of different length. The activity was formulated as percentage (100% corresponds to that of $^{7Me}GpppAC_{20}$).

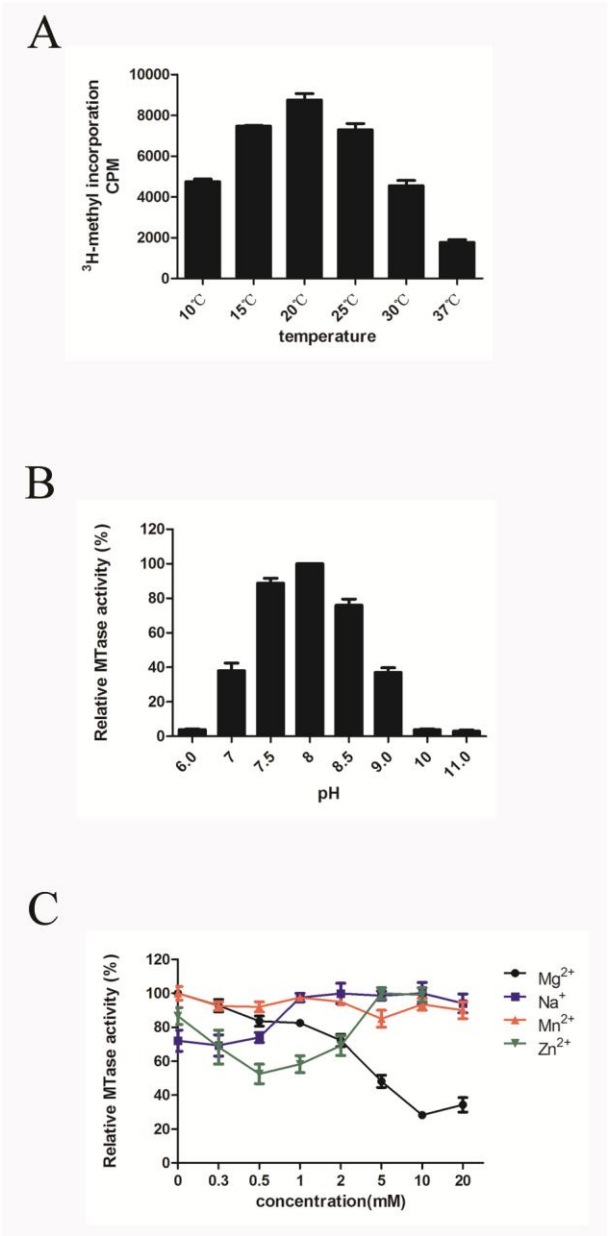

Figure 3. The optimal reaction conditions of GAV nsp16. The GAV nsp16 activity was measured in the presence of ^{3}H-labeled SAM by counting transferred ^{3}H-methyl. (A) Effect of temperature on the enzymatic activity. Reactions were performed in Tris buffer (pH8.0) and incubated at various temperatures. RNAs were purified by Sephadex A-50 and detected by liquid scintillation. (B) Enzymatic activity of GAV nsp16 at different pH values, including citric acid-NaOH (pH6.0), Tris-HCl buffer (pH7.0-9.0), and Na_2CO_3-NaOH buffer (pH10-11). 100% activity corresponds to that at pH8.0. (C) The influence of positive valence metal ions on enzymatic activity. The reactions were conducted at pH8.0 on 20 ℃.

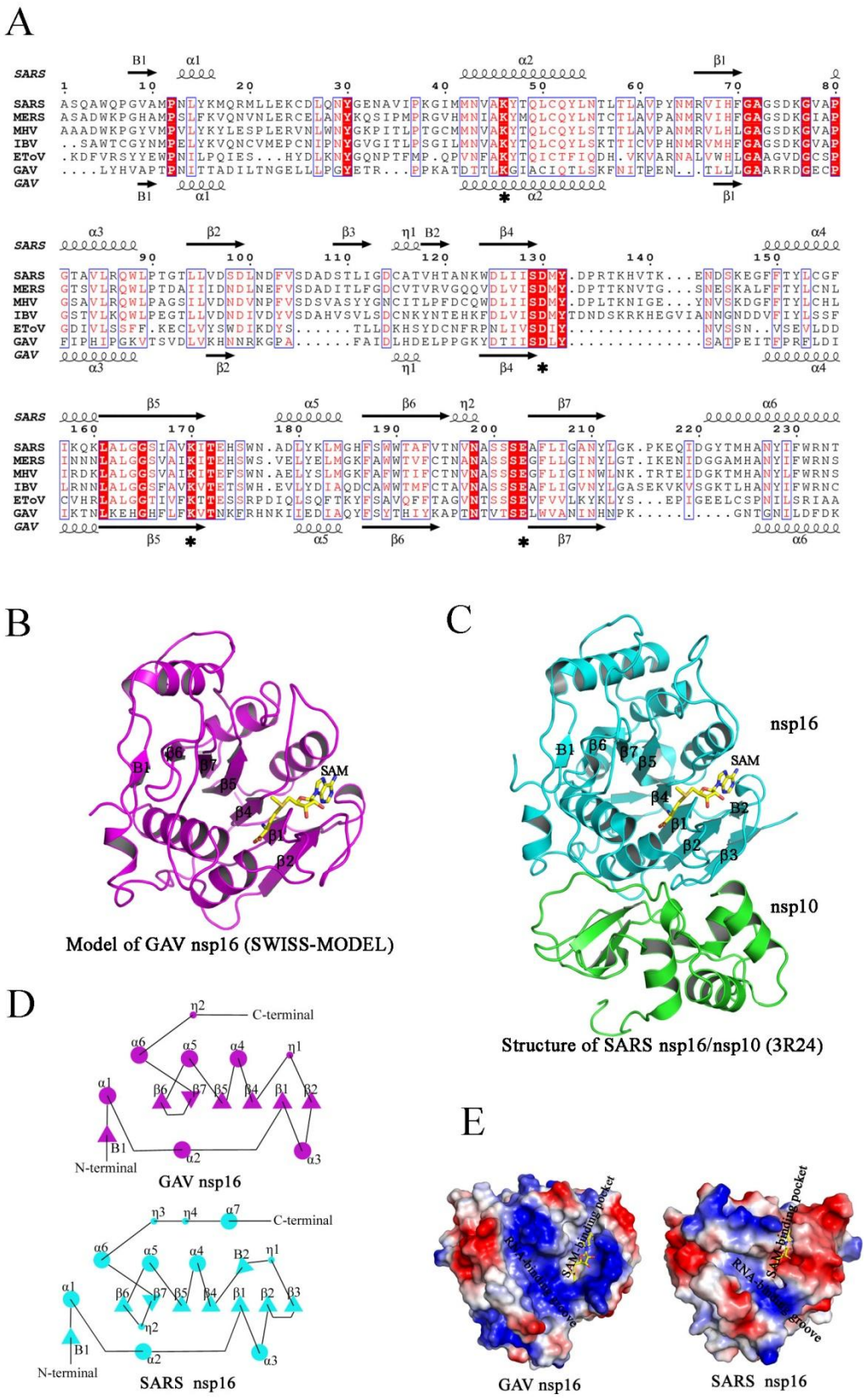

Figure 4. Sequence alignment and homology modeling of GAV nsp16. (A) The multiple sequence alignment of selected 2′-O-methyltransferases of nidoviruses. (B) Ribbon representation of GAV nsp16 model structure generated modeled on the template structure of SARS nsp10/nsp16 (PDB: 3R24) (C). SAM was added in GAV

nsp16 model by superimposition of the model and the structure of SARS nsp10/nsp16 (3R24). β-sheets were marked in accordance with alignment result. (D) Schematic diagrams of the topology of GAV nsp16 (modeled structure) and SARS nsp16. (E) The surface electrostatic potentials of GAV nsp16 (model) and SARS nsp16. Blue areas represent positive charge areas while red represents negative charge areas. RNA-binding groove and SAM-binding pocket are indicated.

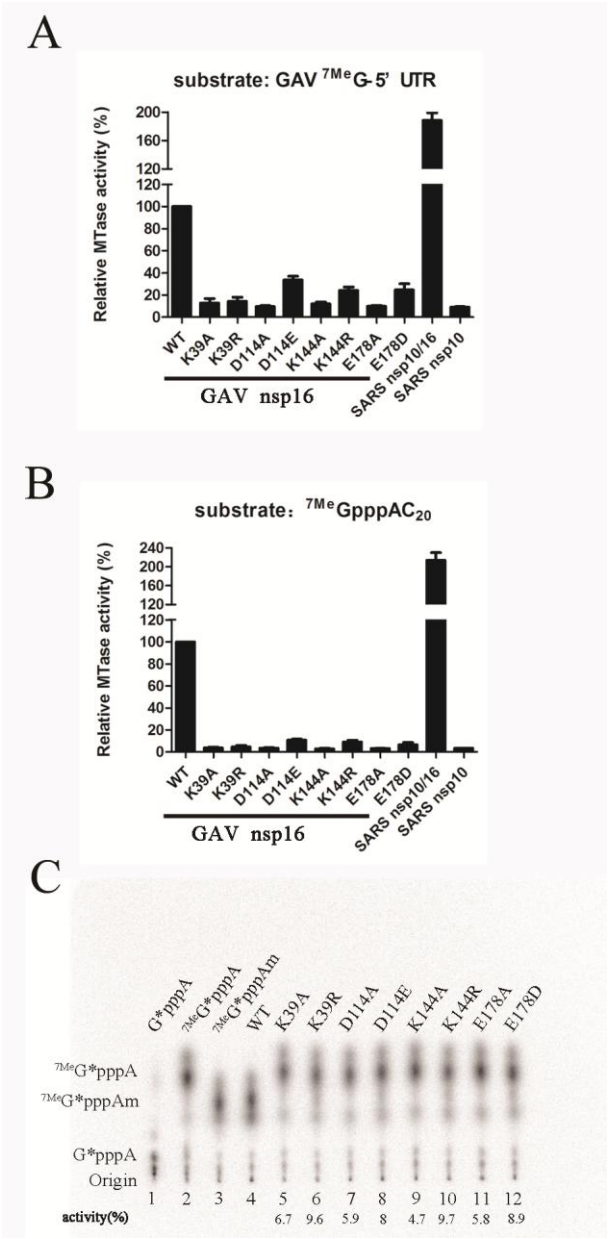

Figure 5. The activity of GAV wild type nsp16 and its K-D-K-E mutants. (A) MTase activity of GAV nsp16 (WT and mutants) detected by using $^{7Me}GpppAC_{20}$ as substrates in ^{3}H-methyl incorporation assay. (B) MTase activity of GAV nsp16 (WT and mutants) detected by using ^{7Me}Gppp-RNA (GAV 5′UTR) as substrates in ^{3}H-methyl incorporation assay. (C) MTase activity of GAV nsp16 (WT and mutants) analyzed by RNA digestion and TLC assays. Lane 4 represents the WT of GAV nsp16, lane 2 as a negative control and lane 3 as positive control treated with vaccinia virus VP39, and the lanes 5-12 are the mutants of GAV nsp16.

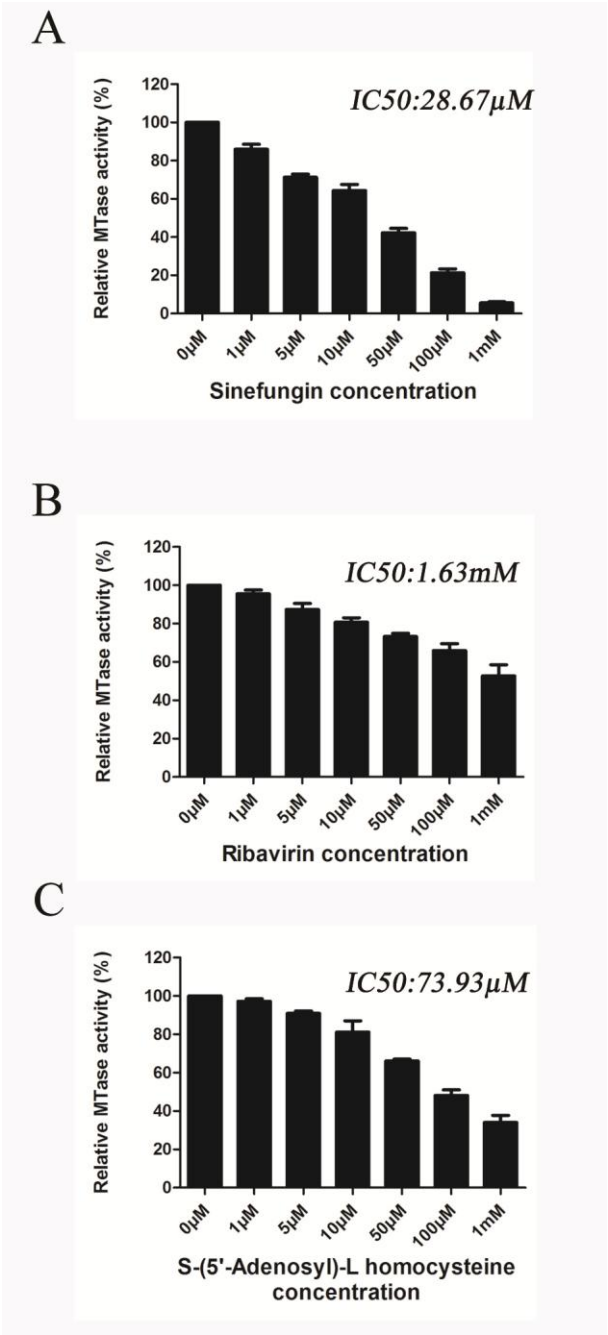

Figure 6. Inhibition of GAV nsp16 2′-O-MTase activity by methyltransferase inhibitors. Increasing concentration of sinefungin (A), ribavirin (B) and AdoHcy (by-product of the reaction) (C) were added in the reaction mixtures, and the activity was measured by using ^{3}H-methyl incorporation MTase activity assays.